Scattering of the fundamental anti-symmetric Lamb wave at delaminations in composite laminates

Ching-Tai Ng and Martin Veidt[a)]
School of Mechanical and Mining Engineering, The University of Queensland, Brisbane, QLD 4072, Australia

(Received 12 April 2010; revised 2 September 2010; accepted 14 December 2010)

An analysis of the scattering characteristics of the fundamental anti-symmetric (A_0) Lamb wave at a delamination in a quasi-isotropic composite laminate is presented. Analytical solutions for this problem do not exist due to the anisotropic nature and multilayer characteristics of composite laminates. This study uses a three-dimensional finite element (FE) method and experimental measurements to provide physical insight into the scattering phenomena. Good agreement is found between simulations and experimental measurements. The results show that the A_0 Lamb wave scattering at a delamination in composite laminates is much more complicated than the scattering at a defect in isotropic plates. Scatter amplitudes and scatter directivity distributions depend on the delamination size to wavelength ratio and the through-thickness location of the delamination damage. The study also investigates the feasibility of the common experimental practice of simulating delamination damage by bonding masses to the surface of composite laminates for guided wave damage detection and characterization methodologies verifications. The results suggest that care is required to use bonded masses to simulate delamination damage for verifying and optimizing damage characterization techniques. In summary, the results of the investigation help to further advance the use of the A_0 Lamb wave for damage detection and characterization.
 [DOI: 10.1121/1.3533741]

PACS number(s): 43.35.Cg, 43.35.Zc [TDM] Pages: 1288–1296

I. INTRODUCTION

In the last two decades, extensive research activities have been carried out in the field of non-destructive evaluation (NDE) to enhance the reliability and reduce the life-cycle costs for current and future infrastructure. Different techniques have been developed utilizing natural frequencies and modeshapes,[1] time domain dynamics responses,[2,3] or guided waves.[4,5] Among the various NDE techniques, Lamb waves have been shown to be sensitive tools to detect most types of defects, efficient in detecting small and subsurface damages and able to inspect large areas.[6,7] The understanding of Lamb waves scattering characteristics plays an important role in the successful application of Lamb waves for damage detection. Different research activities have been conducted to study the interaction of Lamb waves at different types of damage in various materials. A number of developments[8–10] have been achieved for isotropic materials.

In recent years, the use of fiber-reinforced composite laminates has steadily increased in engineering applications, such as aerospace, civil, maritime, and automotive, because of their high specific stiffness, light weight, and corrosion resistance as compared with traditional metallic materials. However, the damages of composite laminates are more critical than those in metallic materials as more damage modes exist (e.g., delamination, matrix cracking, and fiber breakage) and these damages are more difficult to be detected and characterized. Delamination is one of the most common and serious failure modes in composite laminates. It can be caused by low velocity impacts, imperfections during manufacturing process, or fatigue loading. Delamination is a separation of adjacent subsurface laminae without any obvious visual evidence on the surface. For example, delaminations in aircraft structures need to be reported if they are larger than a certain size. The critical size of delamination depends on several factors, in particular, design philosophy and material type. For a carbon fiber-reinforced laminate wing skin of a modern fighter aircraft, the typical critical delamination size is around $10 \times 10\ \text{mm}^2$ for the area exposed to direct airflow.[11] In this study, similar delamination sizes are considered to address the practical situation.

Analytical solutions of Lamb waves scattering at delamination do not exist for composite laminates due to their anisotropic nature and multilayer characteristics. Several studies have been carried out to investigate and understand Lamb wave scattering at delaminations using numerical simulations. Guo and Cawley[6] employed a two-dimensional (2D) finite element (FE) method with plane strain assumption to study the reflection of the fundamental symmetric (S_0) Lamb wave from a delamination in unidirectional and cross ply laminates with experimental verifications. It was shown that the S_0 Lamb wave cannot be used to detect the delamination at the through-thickness locations with zero shear stress. Hayashi and Kawashima[12] studied the reflection characteristics of S_0 and A_0 Lamb waves from a delamination of cross ply laminates using a 2D strip element method. They showed that the A_0 Lamb wave is sensitive to the delamination at all through-thickness locations. Recently, Ramadas *et al.*[13] investigated the A_0 Lamb wave interaction at a delamination located at the middle plane of a composite laminate. An experimentally validated 2D FE model was used to explain

a)Author to whom correspondence should be addressed. Electronic mail: m.veidt@uq.edu.au

the A_0 Lamb wave interaction at delamination. They showed that the S_0 Lamb wave is generated at the leading edge of the delamination due to mode conversion. However, it is confined only to the sub-laminates within the delamination region and converts back to the A_0 Lamb wave when exiting the delamination. The aforementioned studies provided an insight to the fundamental physical phenomena of Lamb waves interaction at a delamination. They also showed that the A_0 Lamb wave is sensitive to the delamination at all through-thickness locations. In addition, because the A_0 Lamb wave has shorter wavelength than S_0 Lamb wave at the same frequency, it is potentially more sensitive to delamination damage. Due to the favorable characteristics of the A_0 Lamb wave, it has attracted interest in the context of damage detection.[4,14–16] However, all the aforementioned studies are limited to 2D situations which consider the delamination to be across the full width of the composite laminates.

The aim of this paper is to determine the low frequency A_0 Lamb wave scattering characteristics at a delamination in a fiber-reinforced composite laminate. Unlike most of the studies in the literature, the delamination considered in this paper is not across the full width of the laminates and hence it represents the three-dimensional (3D) characteristic of a real delamination. Instead of only studying the backward and forward scattering, the study also investigates the scattering characteristics in different directions which are important to the damage detection techniques utilizing a distributed transducer network.[15–18] Numerical simulations using a 3D FE method and experimental measurements were utilized to explore the scattering characteristics of the A_0 Lamb wave at a delamination.

The paper is organized as follows. The 3D FE simulation of a delaminated composite laminate is first described in Sec. II. The details of the experimental investigations are given in Sec. III. Section IV presents the results of the experimental verification of FE simulations. The A_0 Lamb wave scattering characteristics are then discussed in detail by a series of studies in Sec. V. Section VI studies the feasibility of simulating delamination damage using bonded masses. Finally, conclusions are drawn in Sec. VII.

II. FE SIMULATIONS OF DELAMINATED COMPOSITE LAMINATES

A 3D FE method was used to simulate an eight-ply $[45/-45/0/90]_S$ quasi-isotropic composite laminate with a delamination. This stacking sequence has been used for different analysis in previous studies.[19,20] ANSYS[21] was used to generate the geometry and perform the meshing of the FE model. A schematic diagram of the configuration used in FE simulations is shown in Fig. 1(a). Each lamina is modeled using eight-noded 3D reduced integration solid brick elements with hourglass control in which each node has three degrees-of-freedom (DoFs). The lamina is the same as the one used in the experiments, namely, a Cycom® (Tempe, Arizona, USA) 970/T300 unidirectional carbon/epoxy prepreg tape with 0.55 fiber volume fraction, 1517 kg/m^3 density, and 0.2 mm thickness. The effective elastic properties of the lamina were determined from micromechanics theory with the

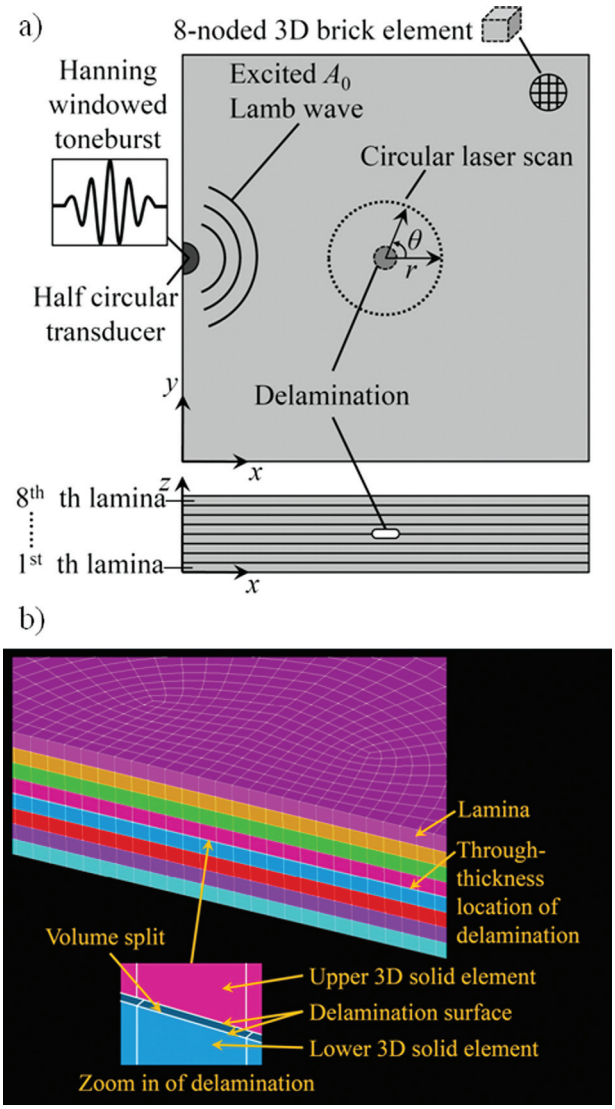

FIG. 1. (Color online) (a) Schematic diagram of the configuration used in FE simulations, (b) 3D FE model cross section at the delamination.

consideration of the constituents[22] and are listed in Table I. A very small and stiffness proportional damping was considered to ensure the numerical stability and simulate the damping effect of the composite materials. As shown in Fig. 1(a), a circular delamination is modeled at the center of the composite laminate. Without loss of generality, the delamination can exist at any through-thickness location. Figure 1(b) shows a cross section at the delamination region in the 3D FE model. The delamination is modeled by a volume split at the delamination region in which the FE nodes across the delamination surfaces are separated by a small distance according to standard FE simulation practice,[6,23] which is supported by experimental observations reported in Sec. III.

Figure 2 shows the theoretical phase velocity dispersion curves for a $[45/-45/0/90]_S$ quasi-isotropic composite laminate in the 0° propagation direction calculated by DISPERSE.[24] It should be noted that there is a small variation of the phase velocity dispersion curves for other directions due to the anisotropic behavior of composite laminate.[25] Apart from the A_0 mode, the S_0 and fundamental shear horizontal (SH_0) modes also exist at the low frequency-thickness

TABLE I. Elastic properties of Cycom® 970/T300 prepreg lamina.

E_{11} (GPa)	E_{22} (GPa)	E_{33} (GPa)	G_{12} (GPa)	G_{13} (GPa)	G_{23} (GPa)	ν_{12}	ν_{13}	ν_{23}	ρ (kg/m^3)
128.75	8.35	8.35	4.47	4.47	2.90	0.33	0.33	0.44	1517

regime. Obviously, the A_0 Lamb wave has much lower phase velocity compared to S_0 and SH_0 which means the wavelength of the A_0 Lamb wave is also much smaller. This makes the A_0 Lamb wave more sensitive to small damages. The excitation signal used in this study is a 140 kHz narrow-band six-cycle sinusoidal tone bust pulse modulated by a Hanning window. The reason of selecting this excitation frequency is that better signal-to-noise ratio can be obtained in the experimental studies which enables easier comparison between the FE simulations and experimental results. The A_0 Lamb wave is generated by applying the out-of-plane nodal displacement to the surface FE nodes covered by the 5 mm diameter circular transducer area as shown in Fig. 1(a). According to the phase velocity dispersion curves in Fig. 2, although the S_0 and SH_0 modes also exist at the low frequency-thickness regime, the applied out-of-plane nodal displacement generates very little in-plane motion. The theoretically calculated wavelength of the A_0 Lamb wave at the excitation frequency is around 8 mm. Solid elements with in-plane square dimensions 0.4×0.4 mm^2 are used through the whole model. This means at least 20 FE nodes exist per wavelength which is twice the minimum number of 10 nodes recommended in the literature to simulate Lamb wave propagation using FE analysis.[15,26] The thickness of each solid element is 0.2 mm, which gives an aspect ratio of two for the solid elements. A convergence study was carried out to confirm that the results of using elements with aspect ratio of two having identical accuracy comparing to cubic elements. The dynamic simulation was solved using the explicit FE code LS-DYNA.[27] LS-DYNA employs an explicit central difference integration scheme, which assumes a diagonal mass matrix to avoid the need for global matrix assembly or inversion in the FE solution, to calculate the response of Lamb waves. The hourglass energy was kept below 2% of the internal energy for all simulations to ensure the accuracy of the elastic wave propagation. The size of the composite laminate varies from case to case and is selected to ensure that the laminate is large enough to avoid the simulated scattering signals contain boundary reflections from the edge in the study. The size of the laminate is in the range of 180–250 mm resulting between 1.62 and 3.13 million elements. Simulations were carried out on a Sun Microsystems (Redwood City, California, USA) X220 cluster with 30 nodes (each node has a dual quad-core AMD Opteron™ processor 2356 at 2.3GHz with 8GB RAM).

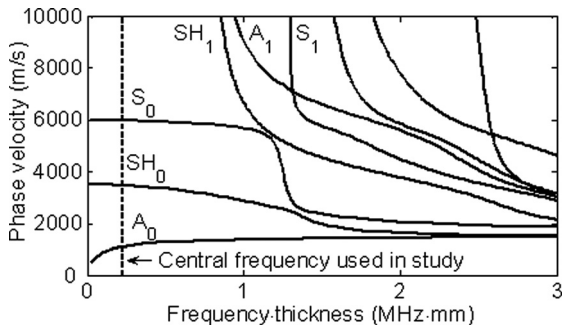

FIG. 2. Phase velocity dispersion curves for the $[45/-45/0/90]_S$ quasi-isotropic composite laminate at 0° propagation direction.

Figure 3 presents typical contour snapshots of FE simulated out-of-plane displacement of the $[45/-45/0/90]_S$ quasi-isotropic laminate. Figure 3(a) shows an instant soon after the excitation in which the A_0 Lamb wave is generated. It shows that the energy flow of the wave is focused along the fiber direction of the two outer layers.[28] This is different to isotropic materials and makes the Lamb waves scattering characteristics more complicated. Figure 3(b) shows the scattered and transmitted wave after the interaction of the incident A_0 Lamb wave with the delamination.

III. EXPERIMENTAL SETUP

A $600 \times 600 \times 1.6$ mm^3 eight-ply $[45/-45/0/90]_S$ delaminated composite laminate was manufactured from the same lamina material as in FE simulations (Cycom® 970/T300

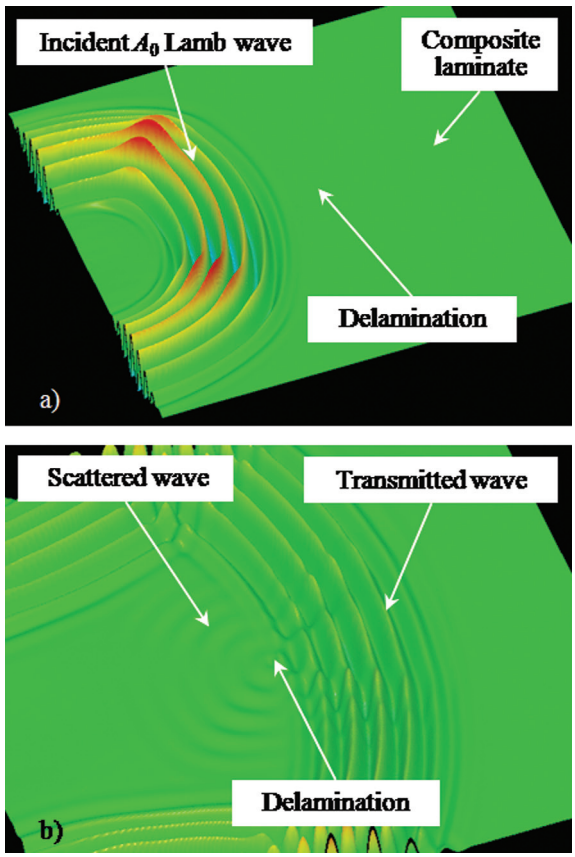

FIG. 3. (Color online) Typical contour snapshots of FE simulated out-of-plane displacement for the $[45/-45/0/90]_S$ composite laminate at different time instances, (a) soon after excitation and (b) shortly after A_0 Lamb wave interaction with a 11 mm diameter circular delamination located between the fourth and fifth lamina.

unidirectional carbon/epoxy prepreg tape). The delamination is circular in shape with 11 mm diameter which is similar to the critical size of delamination in the aircraft industry as discussed in Sec. I. A circular sheet of 11 mm diameter thin fluoropolymer release film was inserted at the center of the laminate between the fourth and fifth lamina during the layup fabrication process. After the laminate was autoclaved, a small flexural load was applied to ensure the separation of the inserted fluoropolymer release film from the laminate. The presence of the delamination was confirmed using ultrasonic C-Scan. In addition, a small sample with the same delamination was also fabricated for microscopic analysis. The sample was cut at the middle of the delamination. The microscopic analysis of the cross section confirmed that the fluoropolymer release film was separated from the laminate resulting in small volume splits around two adjacent laminae as discussed in Sec. II.

A 5 mm diameter and 2 mm thick piezoceramic disc (Ferroperm Pz27) was surface mounted to the composite laminate to excite the A_0 Lamb wave. A 3 mm thick brass mass with the same diameter was used as a backing mass to increase the strength of the excited A_0 Lamb wave.[29] The excitation signal is a 140 kHz narrow-band six-cycle sinusoidal tone burst pulse modulated by a Hanning window, which is identical to the excitation signal used in FE simulations. The required excitation signal was generated by a computer controlled arbitrary waveform generator [Stanford Research DS345 (Sunnyvale, California, USA)] with 10 V peak-to-peak output voltage, and a power amplifier [Krohn Hite model 7500 (Brockton, Massachussets, USA)] was used to amplify the excitation voltage by a factor of 10–50. A Laser Doppler vibrometer [OFV 303/OFV 3001, Polytech GmbH (Waldbronn, Germany)] with the laser head positioned by a computer controlled positioning system [Newport ESP 300 (Irvine, California, USA)] was used for measuring the out-of-plane displacement. A thin reflective tape was attached to the surface of the laminate to enhance the optical backscatter reflection of the laser beam. The measured out-of-plane displacement was then fed into a computer via a Tektronix TDS420A oscilloscope (Portland, Oregon, USA). The quality of the measurements was improved by averaging the signals over 1000 acquisitions and applying a band-pass filter. As shown in Fig. 1(a), the cylindrical coordinate system is at the center of the delamination, and the piezoceramic disc was located at $r = 90$ mm and $\theta = 180°$.

IV. EXPERIMENTAL VERIFICATION

A. Low frequency Lamb wave propagation in composite laminates

This section presents a study of the low frequency A_0 Lamb wave propagation in the $[45/-45/0/90]_S$ quasi-isotropic composite laminate. The FE model described in Sec. II is validated by means of phase velocity of Lamb waves using theoretical and experimental results to ensure that the FE simulations are able to accurately predict the propagation of Lamb waves in composite laminate.

The phase velocity dispersion curves for experimental measurements are obtained by sweeping the excitation frequency from 20 to 300 kHz in steps of 20 kHz. At each excitation frequency, five measurement points were taken along the 0° direction with the distance between measurement points less than one half of the excitation signal wavelength. The distance between the excitation transducer and the first measurement point is 50 mm, i.e. clearly more than the four wavelengths required for the far-field wave field solution to be valid.[10] The phase velocity at each excitation frequency is then calculated by averaging the results of all measurement points. The same strategy was used to obtain the phase velocity dispersion curves for FE simulations. Figure 4(a) shows the phase velocity dispersion curves of both S_0 and A_0 Lamb waves from theoretical calculation using DISPERSE (solid line), FE simulations (empty circles), and experimental measurements (triangles). As the Laser Doppler vibrometer was employed to measure the out-of-plane displacement, the measurement system is mainly sensitive to the A_0 mode since the S_0 and SH_0 waves have very small out-of-plane displacement magnitude at the low frequency regime. Although this study focuses on the A_0 Lamb wave, the theoretical results of both S_0 and A_0 modes are included in the dispersion curves. As shown in Fig. 4(a), there is a very good agreement between the calculated, simulated, and experimental measured phase velocity dispersion curves. It indicates that the FE model is able to predict the Lamb waves propagation accurately.

Figure 4(b) shows the in-plane and out-of-plane displacement modeshape of A_0 mode for the $[45/-45/0/90]_s$ quasi-isotropic composite laminate at $\theta = 0°$ and 140 kHz. Compared to the isotropic case discontinuities exist in the in-plane displacement slopes between the laminae, especially at 0.25 and −0.25 normalized through-thickness location where

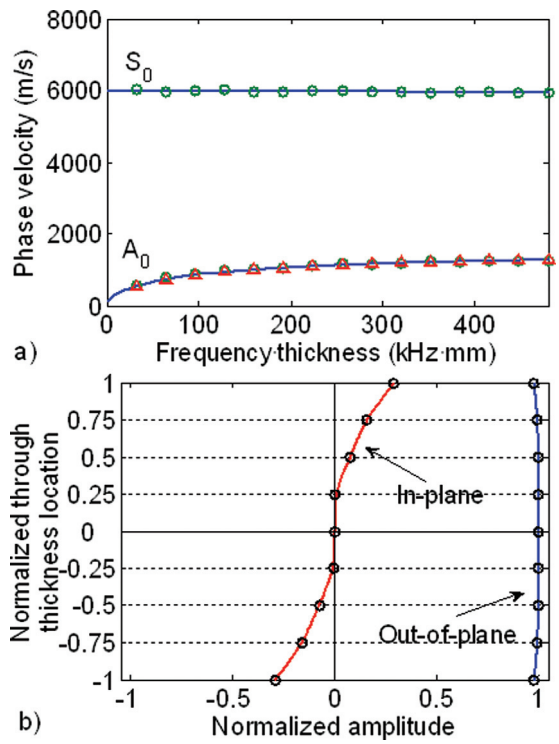

FIG. 4. (Color online) (a) Phase velocity dispersion curves from theoretical calculation (solid lines), FE simulations (circles), and experimental measurements (triangle) for $\theta = 0°$ and (b) displacement modeshapes at 140 kHz (solid lines, theoretical calculation; circle, FE simulations).

the fiber alignment of the adjacent laminae are perpendicular to each other (0° and 90° plies). Excellent agreement is found between the results from theoretical calculation and FE simulations indicating that the FE model accurately predicts the propagation characteristics of the A_0 Lamb wave in composite laminates including through-thickness displacement modeshapes.

B. Reflection and transmission at delamination

The reflection and transmission of the A_0 Lamb wave at a delamination are studied in this section. The FE model described in Sec. II was used to simulate the $[45/-45/0/90]_S$ quasi-isotropic composite laminate with a 11 mm diameter circular delamination (as described in Sec. III) and the results are compared with the experimental measurements. A number of measurements were taken at $r=40$ mm and $140° \leq \theta \leq 220°$ with 10° interval to obtain the reflection wave from delamination. In the case of the transmission wave, the measurements were at the $r=40$ mm for $0° \leq \theta \leq 30°$ and $330° \leq \theta \leq 350°$. Figure 5 shows a typical signal from FE simulation and measured signals at $r=40$ mm and $\theta=220°$ for incident wave with 140 kHz excitation frequency. It shows that there is a very good agreement between the FE simulations and experimental measurements, especially for the incident wave. There exists a small phase shift of the reflection between the FE and experimental scattered wave which may be caused by a small uncertainty in the location of the delamination in the experimental sample. However, the amplitudes of the reflection waves are still in a very good agreement. Figure 5 also shows that a single reflection wave is obtained from the delamination because the delamination size is comparable to the excited A_0 mode wavelength. It can be seen that the reflected wave is completely separated from the incident wave and the same situation can be achieved for all measurements at $140° \leq \theta \leq 220°$. By isolating the incident wave, the maximum absolute amplitude of the reflected wave can thus be determined in the time domain. Figures 6(a) and 6(b) show the maximum absolute amplitude of the reflected and transmitted waves from the delamination, respectively, where the amplitudes of the reflected and transmitted waves are normalized by the amplitude of the incident wave at $r=40$ mm and $\theta=180°$. As shown in Fig. 6(a),

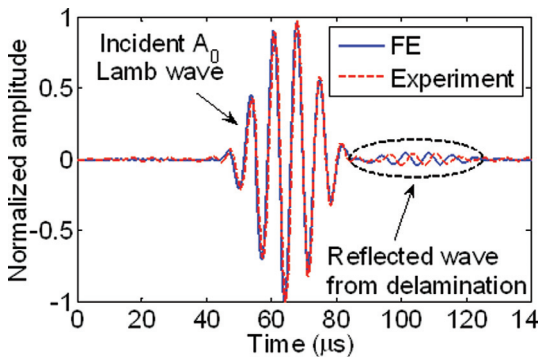

FIG. 5. (Color online) Typical FE simulated and experimental measured time signals at $r=40$ mm, $\theta=220°$ of the composite laminate with a 11 mm diameter circular delamination located between the fourth and fifth lamina.

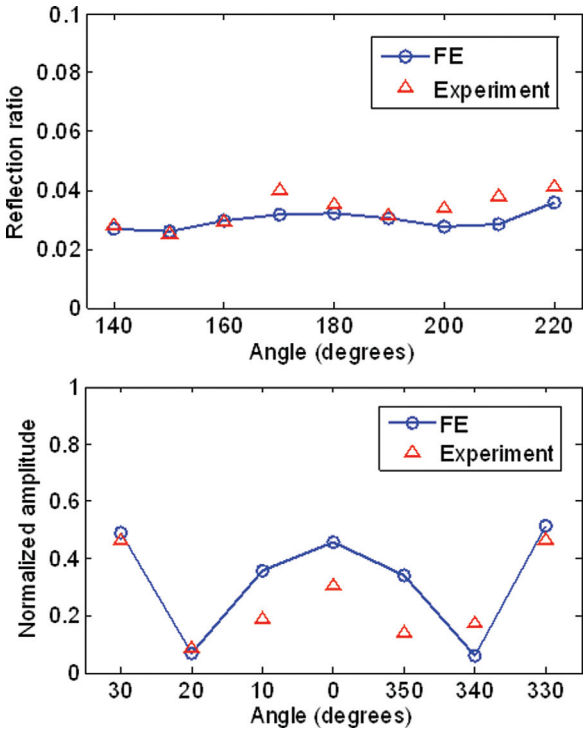

FIG. 6. (Color online) Normalized amplitude of the (a) reflected and (b) transmitted waves from a 11 mm diameter circular delamination located between the fourth and fifth lamina as a function of θ by 140 kHz incident wave.

there is a small discrepancy between the FE simulated and experimental results for the reflected Lamb wave amplitudes. However, the FE simulation still well predicts the experimental results in general. In the case of transmitted wave, a larger discrepancy is observed in Fig. 6(b) which may be caused by the effect of the fluoropolymer release film. It should be noted that although a particular excitation frequency was selected in the study, the FE model is general and can be used for other excitation frequencies provided the number of FE nodes per wavelength requirement is fulfilled.[16,27]

V. SCATTERING DIRECTIVITY PATTERN

Sections IV A and IV B demonstrated that the FE simulations accurately predict the A_0 Lamb wave propagation and scattering at the delamination. This section employs the validated FE model to study the A_0 Lamb wave scattering characteristics at delaminations with different sizes by means of the scattering directivity pattern (SDP). For calculating the SDP, the excitation is at $r=90$ mm and $\theta=180°$ according to the cylindrical coordinate system shown in Fig. 1(a). The out-of-plane displacement of 36 nodal points located at $r=40$ mm and $0° \leq \theta \leq 360°$ with 10° step increments were monitored. This distance fulfils the far-field requirement[10] thus the evanescent waves can be ignored. The through-thickness monitoring location is at the middle plane of the laminate where other possible wave modes, such as S_0 and SH_0, produce zero out-of-plane displacement to guarantee that only the A_0 Lamb wave is obtained. For SDP studies in this section, the scattered wave is extracted by using the

baseline subtraction technique which ensures the scattered wave is completely isolated from the incident wave. This can be achieved by carrying out two simulations with the same meshing for the intact and delaminated laminates. The out-of-plane displacement of the scattered wave $u_{r,\theta}^{(S)}(t)]$ is obtained by

$$u_{r,\theta}^{(S)}(t) = u_{r,\theta}^{(D)}(t) - u_{r,\theta}^{(U)}(t), \tag{1}$$

where $u_{r,\theta}^{(U)}(t)$ and $u_{r,\theta}^{(D)}(t)$ are the out-of-plane displacement components at location (r, θ) for the intact and delaminated laminates, respectively. It should be noted that the calculated displacement at mid-thickness and the measured displacements at the surface are normalized by the out-of-plane displacements of the outgoing excitation pulse at the corresponding through-thickness positions, which helps comparing identical relative changes in the SDP although the through-thickness locations where the data are collected are different. The SDP is then constructed by determining the maximum absolute amplitude of the scattered wave in time domain. Figures 7(a)–7(c) show the SDP of the 140 kHz incident A_0 Lamb wave at the 3, 5, and 11 mm diameter circular delamination located between the fourth and fifth lamina, respectively. It should be noted that all scattering amplitudes are normalized by the maximum absolute amplitude of the incident wave at the delamination center location of the intact laminate.

As a point of interest, the SDP is not symmetric with respect to the 0° direction although the delamination is symmetric. This is different for the case of isotropic materials with a symmetric defect in which the SDP is perfectly symmetric.[9,30,31] It indicates that the SDP of composite laminates is more complicated than that in isotropic materials. The non-symmetric behavior of the SDP is due to the non-symmetric layup for the upper and lower sub-laminate at the delamination region and the non-symmetric distribution of incident wave amplitude [as shown in Fig. 3(a)]. Figure 7 shows that the maximum scattering amplitude increases for larger delamination sizes. The backward and forward scattering amplitudes are of the same order of magnitude for the 3 mm diameter delamination in which the delamination diameter to wavelength ratio at $\theta = 0°$ (R_{DW}) is 0.38. However, the forward scattered components tend to have larger amplitude for larger R_{DW} ($R_{DW} = 0.63$ for 5 mm diameter and $R_{DW} = 1.39$ for 11 mm diameter). The effect of the ratio between the wavelength of the incident wave and the delamination size will be discussed in more detail in Sec. V A. As shown in Fig. 7, the scattering amplitudes around the direction perpendicular to the incident wave have relative small amplitude. In the case of a pitch-catch damage detection approach, it is unlikely that the delamination can be detected if the sensor is located along these directions.

A. Influence of delamination size

It has been demonstrated that the scattering characteristics highly depend on the size of the delamination. This section explores this phenomenon in more detail. Without loss of generality, the study is in terms of R_{DW}. Figure 8(a) shows the forward scattering amplitudes at $\theta = 0°$, 40°, 80°, 280°, and 320° for different R_{DW}. It can be seen that the scattering amplitude aligned in the same direction as the incident wave ($\theta = 0°$) increases with R_{DW} and has the largest amplitude comparing to other θ for R_{DW} larger than around 0.9. The scattering amplitudes at $\theta = 40°$ and 320° rise until the R_{DW} reaches around 1.1 and 1.0, respectively, then reduce with R_{DW}. For $\theta = 80°$ and 280°, the amplitude exhibits a slight variation but the overall trend is a slow increase.

Figure 8(b) shows the backward scattering amplitudes at $\theta = 100°$, 140°, 180°, 220°, and 260°. It is obvious that the phenomenon of the backward scattering amplitudes is quite different to that of forward scattering. For $\theta = 140°$, 180°, and 220°, the amplitude rises almost linearly for R_{DW} larger than 0.25 and then starts falling when R_{DW} is around 0.55. For R_{DW} larger than approximately 0.8 the values fluctuate around a slightly increasing trend line. For $\theta = 100°$ and 260° which are almost perpendicular to the incident wave direction, the major trend is a steady increase with slight variations with amplitudes that are generally smaller than those for $\theta = 140°$, 180°, and 220°. Comparing to Fig. 8(a), it can be seen that the backward scattering amplitudes have larger variations than those of forward scattering and the overall behavior is more complicated and in addition are generally smaller in magnitude than those in forward scattering directions particularly for larger R_{DW} values.

Figure 8(c) shows the backward ($\theta = 180°$) to forward ($\theta = 0°$) scattering amplitude ratio as a function of R_{DW}. It indicates that the backward and forward scattering amplitudes are almost the same for small R_{DW}. However, the forward scattering amplitude continuously becomes larger and is approximately ten times the size of the backward scatter amplitude for R_{DW} larger than 0.7. The trend then exhibits a slight variation around a magnitude of 0.1 over the rest of the considered range of R_{DW}. The phenomenon shown in Fig. 8(c) implies that it is difficult to detect delamination by using damage detection approaches relying mainly on backward scattered wave measurements in the case when the incident

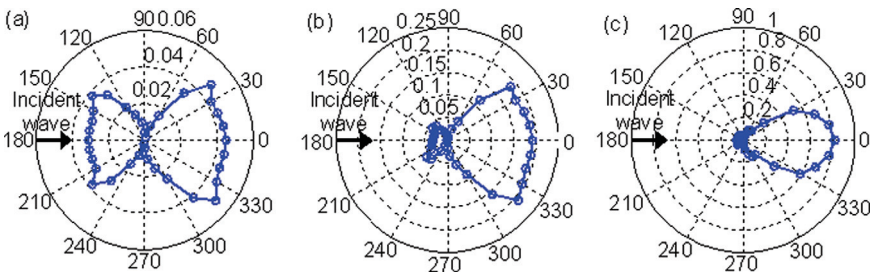

FIG. 7. (Color online) SDP for (a) 3 mm, (b) 5 mm, and (c) 11 mm diameter delaminations located between the fourth and fifth lamina by 140 kHz incident wave.

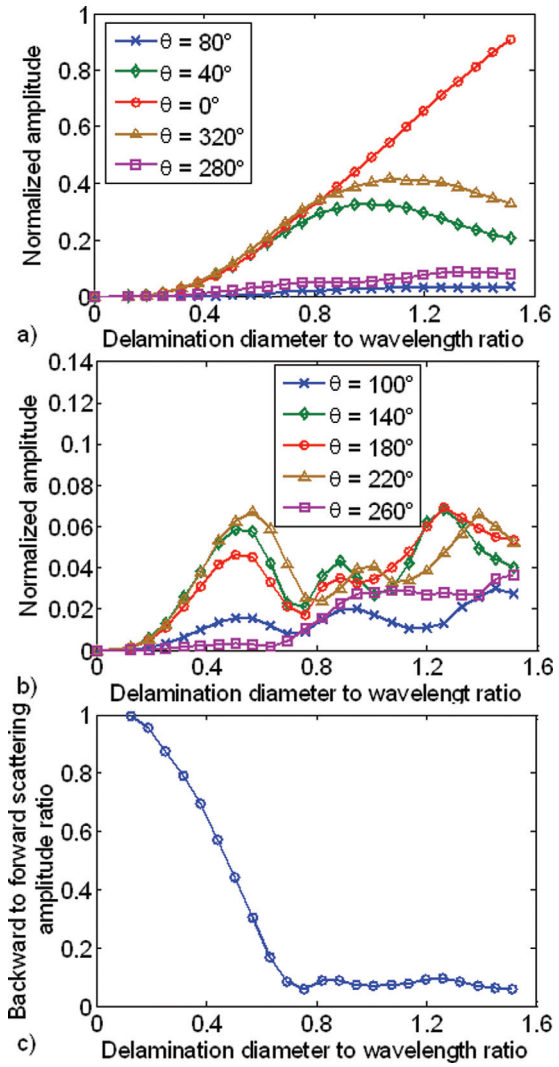

FIG. 8. (Color online) Normalized amplitude for the (a) forward scattering, (b) backward scattering, and (c) backward to forward scattering ratio as a function of delamination diameter to wavelength ratio for delamination located between the fourth and fifth lamina.

A_0 Lamb wave wavelength and delamination size are comparable. A better choice will be those approaches[15,18,32,33] which also utilize the forward scattered wave in a distributed transducer network.

B. Influence of through-thickness location of delamination

The studies in the previous sections show that the scattering characteristics are related to R_{DW}. It is obvious that the SDP also depends on the layup of the laminate and the through-thickness location of the delamination. The delamination causes a local change of the sub-laminate layups at the delamination region due to the separation of adjacent subsurface laminae. Figures 9(a) and 9(b) show the SDP for 5 mm diameter delamination located between the third and fourth, and the second and third lamina for a 140 kHz incident wave, respectively. Comparing Figs. 9(a) and 9(b) with Fig. 7(b) (the same diameter but delamination located between the fourth and fifth lamina), they show that the same diameter delamination at through-thickness locations

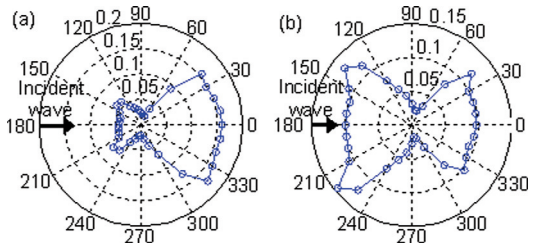

FIG. 9. (Color online) SDP for a 5 mm diameter delamination located between the (a) third and fourth and (b) second and third lamina by 140 kHz incident wave.

has different SDPs. As a point of interest, the forward scattering amplitudes are dominant for delamination between the fourth and fifth lamina. However, the scattering amplitudes are redistributed from forward to backward if the delamination is located between the third and fourth lamina. In the case of delamination located between the second and third lamina, the forward and backward scattering amplitudes have the same order of magnitude. The sensitivity of the SDPs on the through-thickness location of the delamination illustrates that scattering characteristics in composite laminates are in general much more complicated than for defects in isotropic materials.

VI. DELAMINATION SIMULATED BY BONDED MASSES

The results of the study show that the A_0 Lamb wave scattering at a delamination is a complicated phenomenon. In the literature, delaminations are frequently simulated by bonding masses to the surface of laminates for experimental verification of damage detection methods.[17,18,32] As discussed in Sec. V B, the delamination causes a local change of the layup of the laminate at the delamination region due to the separation of adjacent subsurface laminae. It is an open question whether or not delaminations can be well represented by bonding masses to the surface of laminates. This section investigates the SDP of bonded masses attached to the $[45/-45/0/90]_S$ quasi-isotropic composite laminate. The results are then compared with the SDP of delamination cases. The FE model for a bonded mass is first validated using experimental measurements. Cylindrical bonded masses of 5 mm diameter with 3 mm thickness (the bonded mass diameter to wavelength ratio R_{BW} is 0.63) and 10 mm diameter with 5 mm thickness ($R_{BW} = 1.26$) were used in the experiment. The material of the bonded mass is brass. Each bonded mass was surface mounted to one side of the composite laminate and two series of measurements were carried out for the laminate with and without the bonded mass. The SDP was then constructed by using baseline subtraction. In the case of FE simulations, bonded masses were simulated by 3D solid elements according to the geometric and material properties used in the experiment. Figure 10 shows SDP from both FE simulations and experimental measurements. It can be seen that there is good agreement between the FE and experimental results. This indicates that the FE simulations accurately predict the SDP of a bonded mass. A small discrepancy in forward scattering directions may be caused

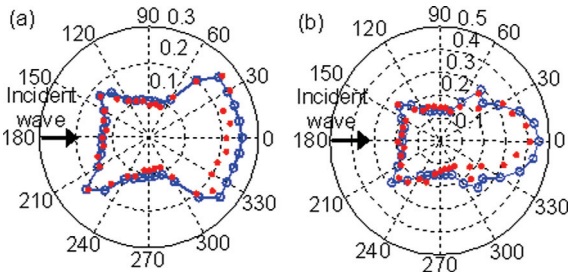

FIG. 10. (Color online) SDP for cylindrical bonded mass of (a) 5 mm diameter with 3 mm thickness, (b) 10 mm diameter with 5 mm thickness from FE simulations (lines with empty circles) and experimental measurements (filled circles) by 140 kHz incident wave.

by the effect of the adhesive layer between the bonded mass and the laminate, which is not modeled in FE simulations.

The following study considers bonded masses with a diameter comparable to the wavelength of the incident wave. 5 mm diameter bonded masses with different thicknesses were selected. Figure 11 shows the scattering amplitudes as a function of θ for 5 mm diameter delaminations at different through-thickness locations and bonded masses with different thicknesses at one side of the laminate. The amplitude is normalized by the maximum absolute amplitude of the incident wave at the delamination and bonded mass center of the intact laminate. Solid, dash, and dash–dot lines represent 5 mm diameter delaminations located between the second and third, third and fourth, and fourth and fifth lamina, respectively. The scattering amplitudes for 5 mm diameter bonded masses with different thicknesses are indicated by solid lines with different markers. Generally, the scattering amplitudes of bonded masses are larger than those of delaminations. Comparing the scattering amplitudes of bonded masses with different thicknesses, the bonded mass with 0.5 mm thickness has a better agreement to delaminations. Figure 11 also shows that the backward scattering amplitudes of 0.5 mm thickness bonded mass are closer to that of delamination located between the second and third lamina, whereas in the case of forward scattering, the amplitudes are closer to that of delamination located in the mid-plane.

As a representative example, Fig. 12 shows the normalized amplitude as a function of damage diameter to wavelength ratio for $\theta = 0°$ and 180°. They show comparisons of the scattered wave amplitude from delamination damage at different through-thickness locations and bonded masses attached to one side of the laminate, respectively. It can be seen that the scattered wave amplitudes from delaminations and bonded masses are quite different over the entire range of diameter to wavelength ratios. The same is true for $\theta = 40°$, 140°, 220°, and 320°, as well as in the case of bonded masses attached to both sides of the laminate. However, the latter are not shown due to space limitation. These results suggest that simulating delamination damage by bonded masses with the same in-plane dimensions is not as straight forward as suggested in the literature since their SDPs are largely different in amplitude as well as angular distribution. Care is required to select a bonded mass that provides the same SDP as the delamination damage under investigation.

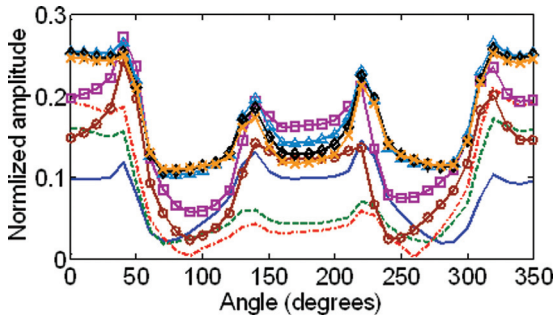

FIG. 11. (Color online) Normalized scattering amplitudes as a function of θ for a 5 mm diameter delamination at different through-thickness locations (solid line, second and third; dash line, third and fourth; dash–dot line, fourth and fifth) and bonded mass with different thicknesses (circle, 0.5 mm; square, 1 mm; triangle, 3 mm; rhombus, 5 mm; cross, 7 mm) at one side of the laminate from FE simulations.

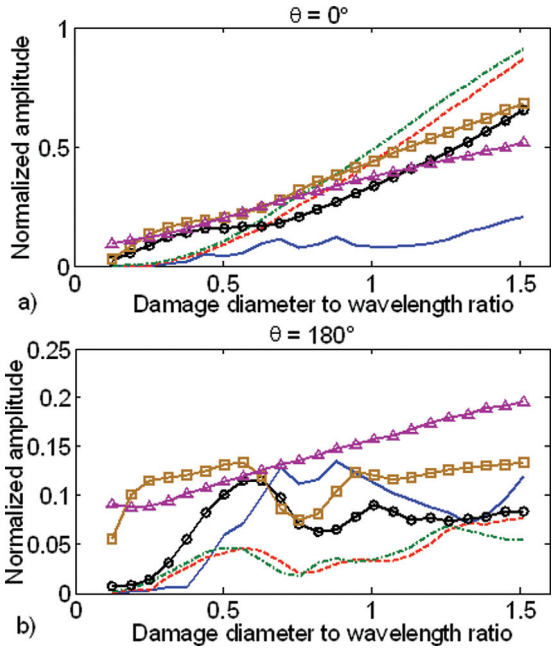

FIG. 12. (Color online) Normalized amplitude as a function of damage diameter to wavelength ratio for $\theta = 0°$ and 180° (solid line, delamination between the second and third lamina; dash line, delamination between the third and fourth lamina; dash–dot line, delamination between the fourth and fifth lamina; circles, 0.5 mm thickness; squares, 1 mm thickness; triangles, 3 mm thickness bonded mass).

VII. CONCLUSIONS

This paper studied the A_0 Lamb wave scattering characteristics at delamination in a $[45/-45/0/90]_S$ quasi-isotropic composite laminates at the low frequency regime. It was demonstrated that explicit 3D FE simulations can accurately predict Lamb waves propagation and their scattering characteristics at delamination damage. Good agreement between FE simulations and experimental measurements was achieved.

Extended parameter studies showed that the A_0 Lamb wave scattering characteristics are substantially more complicated than the case of scattering at defects in isotropic plates. The SDP is not symmetric with respect to the 0° direction even for symmetric delamination geometries due

to the non-symmetric layup of the sub-laminates in the delamination region and the non-symmetric amplitude distribution of the incident wave. The results also show that the behavior of the backward scattering amplitude is generally more complicated than that of the forward scattering amplitude and is generally smaller in magnitude particularly for larger R_{DW} values. In the case of small delaminations both forward and backward scattering amplitudes are of the same order of magnitude. However, forward scattering dominates for larger R_{DW}. In the case of the same delamination size, the scattering amplitude and SDP also depend on the through-thickness location of the delamination. The results of these studies provide improved physical insight into the scattering phenomena at delaminations which can be used to validate and improve the performance of guided wave damage detection methods by selecting transducer locations and excitation frequency and hence help to further advance the use of *in-situ* transducer networks for damage detection and characterization.

A comparison between the scattering amplitudes of surface mounted bonded masses and delaminations showed that the quantitative characteristics are quite different. This suggests that care is required to use bonded masses to simulate delamination damage for verifying and optimizing damage characterization techniques.

ACKNOWLEDGMENTS

C.-T.N. would like to acknowledge the financial support from the University of Queensland and Cooperative Research Centre for Advanced Composite Structures (CRC-ACS). The work has been carried out as part of the CRC-ACS research program. Computational (and/or data visualization) resources used in this work were provided by the Queensland Cyber Infrastructure Foundation. The work was also supported by the Australian Research Council under Discovery Project DP0771585.

[1]H. F. Lam and C. T. Ng, "The selection of pattern features for structural damage detection using an extended Bayesian ANN algorithm," Eng. Struct. **30**, 2762–2770 (2008).
[2]C. P. Fritzen, D. Jennewein, and T. Kiefer, "Damage detection based on model updating methods," Mech. Syst. Signal Process. **12**, 163–186 (1998).
[3]H. F. Lam, C. T. Ng, and M. Veidt, "Experimental characterization of multiple cracks in a cantilever beam utilizing transient vibration data following a probabilistic approach," J. Sound Vib. **305**, 34–49 (2007).
[4]K. Diamanti, C. Soutis, and J. M. Hodgkinson, "Piezoelectric transducer arrangement for the inspection of large composite structures," Composites, Part A **38**, 1121–1130 (2007).
[5]C. T. Ng, M. Veidt, and H. F. Lam, "Guided wave damage characterization in beams utilizing probabilistic optimization," Eng. Struct. **31**, 2842–2850 (2009).
[6]N. Guo and P. Cawley, "The interaction of Lamb waves with delaminations in composite laminates," J. Acoust. Soc. Am. **94**, 2240–2246 (1993).
[7]J. L. Rose, "A baseline and vision of ultrasonic guided wave inspection potential," J. Pressure Vessel Technol. **124**, 273–282 (2002).
[8]M. J. S. Lowe, P. Cawley, J. Y. Kao, and O. Diligent, "The low frequency reflection characteristics of the fundamental antisymmetic Lamb wave a_0 from a rectangular notch in a plate," J. Acoust. Soc. Am. **112**, 2612–2622 (2002).
[9]F. B. Cegla, A. Rohde, and M. Veidt, "Analytical prediction and experimental measurement for mode conversion and scattering of plate waves at non-symmetric circular blind holes in isotropic plate," Wave Motion **45**, 162–177 (2008).
[10]L. Moreau and M. Castaings, "The use of an orthogonality relation for reducing the size of finite element models for 3D guided waves scattering problems," Ultrasonics **48**, 357–366 (2008).
[11]C. Nageswaran, C. R. Bird, and R. Takahashi, "Phased array scanning of artificial and impact damage in carbon fiber reinforced plastic (CFRP)," Insight **48**, 155–159 (2006).
[12]T. Hayashi and K. Kawashima, "Multiple reflections of Lamb waves at a delamination," Ultrasonics **40**, 193–197 (2002).
[13]C. Ramadas, K. Balasubramaniam, M. Joshi, and C. V. Krishnamurthy, "Interaction of the primary anti-symmetric Lamb mode (A_0) with symmetric delaminations: Numerical and experimental studies," Smart Mater. Struct. **18**, 1–7 (2009).
[14]P. Belanger and P. Cawley, "Feasibility of low frequency straight-ray guided wave tomography," NDT & E Int. **42**, 113–119 (2009).
[15]C. T. Ng and M. Veidt, "A Lamb-wave-based technique for damage detection in composite laminates," Smart Mater. Struct. **18**, 1–12 (2009).
[16]C. T. Ng, M. Veidt, and N. Rajic, "Integrated piezoceramic transducers for imaging damage in composite laminates," Proc. SPIE **7493**, 1–8 (2009).
[17]J. B. Ihn and F. K. Chang, "Pitch-catch active sensing methods in structural health monitoring for aircraft structures," Struct. Health Monit. **7**, 5–15 (2008).
[18]C. H. Wang, J. T. Rose, and F. K. Chang, "A synthetic time-reversal imaging method for structural health monitoring," Smart Mater. Struct. **13**, 415–423 (2004).
[19]C. G. Kim and E. J. Jun, "Impact resistance of composite laminated sandwich plates," J. Comput. Math. **26**, 2247–2261 (1992).
[20]C. F. Liu, Y. T. Lee, and H. S. Jou, "A modified finite element smearing technique for free-edge stress analysis," Mech. Adv. Mater. Struct. **5**, 279–289 (1998).
[21]ANSYS 12.0., Meshing and Modeling Guide (ANSYS Inc., 2009).
[22]C. C. Chamis, "Mechanics of composite materials: Past, present and future," J. Compos. Technol. Res. **11**, 3–14 (1989).
[23]S. Takeda, S. Minakuchi, Y. Okabe, and N. Takeda, "Delamination monitoring of laminated composites subjected to low-velocity impact using small-diameter FBG sensors," Composites, Part A **36**, 903–908 (2005).
[24]B. Pavlakovic and M. J. S. Lowe, *DISPERSE: A System for Generating Dispersion Curves, User's Manual Version 2.0.16B* (Imperial College, University of London, London, 2003).
[25]Y. Li and R. B. Thompson, "Influence of anisotropy on the dispersion characteristics of guided ultrasonic plate modes," J. Acoust. Soc. Am. **87**, 1911–1931 (1990).
[26]D. Alleyne and P. Cawley, "The interaction of Lamb waves with defects," IEEE Trans. Ultrason. Ferroelectr. Freq. Control **39**, 381–397 (1992).
[27]LS-DYNA, Version 971 Keyword User's Manual Volume 1 (Livermore Software Technology Corporation, 2007).
[28]C. Potel, S. Baly, J. F. de Belleval, M. J. S. Lowe, and P. Gatignol, "Deviation of a monochromatic Lamb wave beam in anisotropic multilayered media: Asymptotic analysis, numerical and experimental results," IEEE Trans. Ultrason. Ferroelectr. Freq. Control **52**, 987–1001 (2005).
[29]T. Liu, M. Veidt, and S. Kitipornchai, "Single mode Lamb waves in composite laminated plates generated by piezoelectric transducer," Comput. Struct. **58**, 381–396 (2002).
[30]C. Vemula and A. N. Norris, "Flexural wave propagation and scattering on thin plates using Mindlin theory," Wave Motion **26**, 1–12 (1997).
[31]T. Grahn, "Lamb wave scattering from a circular partly through-thickness hole in a plate," Wave Motion, **37**, 63–80 (2003).
[32]H. Sohn, G. Park, J. R. Wait, N. P. Limback, and C. R. Farrar, "Wavelet-based active sensing for delamination detection in composite structures," Smart Mater. Struct. **13**, 153–160 (2004).
[33]L. R. F. Rose and C. H. Wang, "Mindlin plate theory for damage detection: Imaging of flexural inhomogeneities," J. Acoust. Soc. Am. **127**, 754–763 (2010).